RSC Advances

PAPER

View Article Online
View Journal | View Issue

Cite this: *RSC Adv.*, 2017, **7**, 5642

'Aggregation induced emission' active iridium(III) complexes with applications in mitochondrial staining†

Parvej Alam,[a] Subhra Dash,[b] Claudia Climent,[c] Gurpreet Kaur,[d] Angshuman Roy Choudhury,[d] David Casanova,[e] Pere Alemany,[c] Rajdeep Chowdhury*[b] and Inamur Rahaman Laskar*[a]

Received 6th October 2016
Accepted 1st December 2016

DOI: 10.1039/c6ra24792j

www.rsc.org/advances

Two new bis-cyclometalated iridium(III) complexes, $[Ir(F_2ppy)_2(L)]$ and $[Ir(ppy)_2(L)]$, where F_2ppy = 2-(2′,4′-difluoro)phenylpyridine, ppy = 2-phenylpyridine and L = 1,2-((pyridin-2-ylimino)methyl)phenol, have been designed and synthesized by a convenient route. We have univocally characterized their structure by ^1H NMR, ^{19}F NMR, HRMS and SXRD. Both complexes exhibit strong 'Aggregation Induced Emission (AIE)' activity, which has been investigated using spectroscopy measurements, *ab initio* quantum chemical calculations and by analysing their crystal packing. One of the complexes has been shown to have a potential application as a non-toxic bio-imaging probe for mitochondrial staining.

Introduction

Mitochondria, the power houses of cells, are eminent for energy production and apoptosis regulation.[1,2] The organelles found in all eukaryotic organisms are the central hub for many other processes such as lipid modification, redox balance, calcium balance, cellular differentiation, the cell cycle, and innate immunity. In addition, reactive oxygen species (ROS) such as peroxides, the superoxide anion, the hydroxyl radical or singlet oxygen are important cellular signaling species produced by mitochondria.[3,4] These ROS are also associated with several human diseases such as osteoporosis,[5] Alzheimer disease,[6] bowel disease[7] or cardiovascular diseases.[8] According to the recent studies, the morphological change in mitochondria can be affected by the protein involved in apoptosis.[9–13] Hence, the specific imaging of mitochondria has a great importance in the biomedical field. The usual dyes employed for mitochondria imaging are rhodamine 123, Janus green B, Mito Tracker® and Green FM (MTG).[14] Unfortunately, all these dyes suffer from a poor photostability, small Stokes shifts, short fluorescence lifetimes and the accompanying concentration-quenching effect. All these facts boosted the search for efficient solid emitters that could alleviate all these problems for such an application.

Solid state luminescent materials have attracted a great deal of attention from the scientific community because of their many practical applications. Unfortunately, the majority of known luminescent materials are highly emissive in solution while becoming much less emissive or non emissive at all in solid state. This is a quite common effect observed for many luminescent molecules that has been termed 'Aggregation Caused Quenching (ACQ)'[15] in the literature and has been a great obstacle that has greatly limited the development of solid state applications for many luminophores. In 2001, Tang and co-workers discovered a material that exhibited exactly the contrary behavior: while it was highly emissive in the solid state it showed no fluorescent emission at all when dissolved in common organic solvents.[16] This fantastic effect was termed 'Aggregation Induced Emission (AIE)', and it was immediately recognized that it could open the door to a brand new platform for efficient solid state emitters. Worldwide many researchers have been working enthusiastically on the design and synthesis of new AIE materials and their applications.[17–19] In spite of all these efforts, the mechanism behind AIE is only partially understood and a vivid debate is still ongoing in the literature. The field has been recently reviewed by Tang and co-workers.[20] Probably, the most accepted mechanism for AIE is the restriction of internal motion (RIM) and particularly the restriction of internal rotations.[21] Although this mechanism has found to

[a]*Department of Chemistry, Birla Institute of Technology and Science, Pilani Campus, Pilani, Rajasthan, India. E-mail: ir_laskar@bits-pilani.ac.in*

[b]*Department of Biology, Birla Institute of Technology and Science, Pilani Campus, Pilani, Rajasthan, India. E-mail: rajdeep.chowdhury@pilani.bits-pilani.ac.in*

[c]*Departament de Ciència de Materials i Química Física and Institut de Química Teòrica i Computacional (IQTCUB), Universitat de Barcelona, Martí i Franquès 1-11, Barcelona 08028, Spain. E-mail: p.alemany@ub.edu*

[d]*Department of Chemical Sciences, Indian Institute of Science Education and Research (IISER), Sector 81, S. A. S. Nagar, Manauli PO, Mohali, Punjab, 140306, India. E-mail: angshurc@iisermohali.ac.in*

[e]*Kimika Fakultatea, Euskal Herriko Unibertsitatea (UPV/EHU), Donostia International Physics Center, Paseo Manuel de Lardiazabal, 4, Donostia 20018, Euskadi, Spain*

† Electronic supplementary information (ESI) available: Crystal data for complex **2**. CCDC 1505831. For ESI and crystallographic data in CIF or other electronic format see DOI: 10.1039/c6ra24792j

explain the AIE effect in many cases, it has been shown that it cannot explain the emergence of AIE for all known AIE-active molecules and alternative, more specific mechanisms have been proposed in some cases. Apart from RIM, the appearance of AIE is sometimes explained based on the transition to an intramolecular charge transfer (ICT)[22] or twisted intramolecular charge transfer (TICT)[23] state, a *cis–trans* isomerisation,[24] molecular planarization,[25] or the formation of J-type aggregates.[20,26–31]

Besides the development of new organic AIE materials and their applications, the last decade has been dedicated to the development of efficient solid state emitting materials, especially heavy metal complexes[20,32,33] showing phosphorescence instead of fluorescence. Among those heavy metal luminescent compounds, Ir(III) complexes are renowned for their potential applications in the fields of organic light-emitting diodes (OLEDs),[34,35] bioimaging,[36,37] chemosensors[38,39] and vapoluminescent[40] materials because of their superior photophysical properties, long luminescence lifetimes (100 ns to ms), high quantum yields and large Stokes shifts (hundreds of nm).[41] Recently, our group has developed a variety of AIE active iridium(III) based metal complexes.[42–45] Despite all this efforts, the overall development of efficient solid state emitting iridium(III) complexes is still limited and much more work is needed in this direction.

In this report, we have synthesized two new AIE active Ir(III) based complexes (**1** and **2**), which belong to the same family of compounds synthesized by Li *et al.*[46,47] and by S. Y. Park and co-workers.[48] Complex **2** has been used for specific mitochondrial imaging and the MTT cytotoxicity study has been carried out.

Experimental section

Characterization

^{1}H NMR and ^{19}F NMR spectra were recorded in a 400 MHz Brucker spectrometer using $CDCl_3$ as solvent and tetramethylsilane (TMS, $\delta = 0$ for ^{1}H and ^{13}C NMR) as internal standard. UV-vis absorption spectra were recorded in a Shimadzu Spectrophotometer (model UV-1800). The emission spectra were recorded in a Horiba Jobin Yvon (Fluoro Max-4) Spectrofluorometer. Quantum efficiency (QE) in solution was measured with respect to coumarin 153 (in degassed ethanol, QE = 0.38, excitation; 420 nm). The solid state quantum yield for the film samples was measured using a calibrated integrating sphere in a Gemini Spectrophotometer (model Gemini 180). Particle sizes of the nano-aggregates were determined on a Malvern Zetasizer (MAL1040152).

Materials and method

Iridium(III) chloride hydrate and 2-ethoxyethanol were purchased from the Sigma Aldrich Chemical Company Ltd. The 2-(2,4-difluorophenyl)pyridine (F_2ppy) and the bridged complexes ($[Ir(ppy)_2(\mu\text{-}Cl]_2$ and $[Ir(F_2ppy)_2(\mu\text{-}Cl]_2$) were prepared according to the procedure reported in the literature.[45] The ligand (L), 2-((pyridin-2-ylimino)methyl)phenol was synthesized as indicated in ref. 21. The UV-vis grade solvents (DCM, hexane, ethyl acetate) were procured from Merck Company.

Computational details

Electronic structure calculations have been performed within the density functional theory (DFT) framework with the B3LYP energy functional,[49] a basis set of double-ζ quality (LANL2DZ) and the effective core potential of Hay and Wadt for iridium, while the standard 6-31G(d) basis set was used for the rest of atoms in the complex.[50–52] All calculations have been done with the Gaussian program.[53]

General syntheses of $[Ir(F_2ppy)_2L]$, 1 and $[Ir(ppy)_2L]$, 2

In a two-necked round bottom flask (50 mL), 2-((pyridin-2-ylimino)methyl)phenol [L] (0.261 mmol), $[Ir(F_2ppy)_2(\mu\text{-}Cl)]_2$ (or $[Ir(ppy)_2(\mu\text{-}Cl)]_2$ (0.087 mmol), and Na_2CO_3 (0.261 mmol) were mixed in 10 mL of 2-ethoxy ethanol. The mixture was heated at 135 °C for 3 hours under an atmosphere of N_2 gas. The solution mixture was evaporated to dryness and the residue purified by column chromatography using MeOH–DCM–hexane (10 : 90) as the eluent, getting a yellow/red solid product (Scheme 1).

2-((Pyridin-2-ylimino)methyl)phenol (L). ^{1}H NMR (400 MHz, $CDCl_3$) δ 9.46 (s, 1H), 8.53 (ddd, $J = 4.8, 1.9, 0.8$ Hz, 1H), 7.86–7.70 (m, 1H), 7.52 (dd, $J = 7.7, 1.7$ Hz, 1H), 7.43 (ddd, $J = 8.4, 7.3, 1.7$ Hz, 1H), 7.34 (dt, $J = 7.9, 0.9$ Hz, 1H), 7.24 (ddd, $J = 7.4, 4.8, 1.1$ Hz, 1H), 7.09–7.02 (m, 1H), 6.97 (td, $J = 7.6, 1.1$ Hz, 1H). ESI-HRMS (electrospray ionization coupled with high-resolution mass spectrometer) calculated: $C_{12}H_{11}N_2O$ ($[M + H]^+$): *m*/*z*, 199.0871, found; ($[M + H]^+$): *m*/*z*, 199.1184, yellow solid; yield, 80.00% (Fig. S1†).

Complex 1. ^{1}H NMR (400 MHz, $CDCl_3$) δ 9.19 (dd, $J = 5.8$, 0.9 Hz, 1H), 8.87 (dd, $J = 5.8$, 0.9 Hz, 1H), 8.36–8.22 (m, 2H), 8.19–8.07 (m, 2H), 7.88–7.64 (m, 2H), 7.38–7.25 (m, 1H), 7.26–7.13 (m, 4H), 6.87 (ddd, $J = 7.4, 4.9, 0.9$ Hz, 1H), 6.77 (d, $J = 8.7$ Hz, 1H), 6.46 (ddd, $J = 7.9, 6.8, 1.0$ Hz, 1H), 6.38 (ddd, $J = 12.5, 9.2, 2.4$ Hz, 1H), 6.11 (ddd, $J = 12.4, 9.3, 2.3$ Hz, 1H), 5.87 (d, $J = 8.0$ Hz, 1H), 5.59 (dd, $J = 8.6, 2.4$ Hz, 1H), 5.53 (dd, $J = 8.9, 2.3$ Hz, 1H). ^{19}F NMR (376 MHz, $CDCl_3$) δ −108.67, −108.70, −109.51, −109.53, −110.89, −110.92, −111.75, −111.77.

ESI-HRMS calculated: $C_{34}H_{22}F_4IrN_4O$ ($[M + H]^+$): *m*/*z*, 771.1359, found; ($[M + H]^+$): *m*/*z*, 771.1331, pale yellow solid; yield, 65.00% (Fig. S2†).

Complex 2. ^{1}H NMR (400 MHz, $CDCl_3$) δ 9.19 (d, $J = 5.4$ Hz, 1H), 8.90 (d, $J = 5.7$ Hz, 1H), 8.35 (s, 1H), 8.10 (d, $J = 4.8$ Hz, 1H), 7.86 (d, $J = 8.1$ Hz, 1H), 7.79–7.65 (m, 3H), 7.59 (d, $J = 7.7$ Hz, 1H), 7.33–7.22 (m, 1H), 7.20–7.16 (m, 1H), 7.17–7.08 (m, 1H),

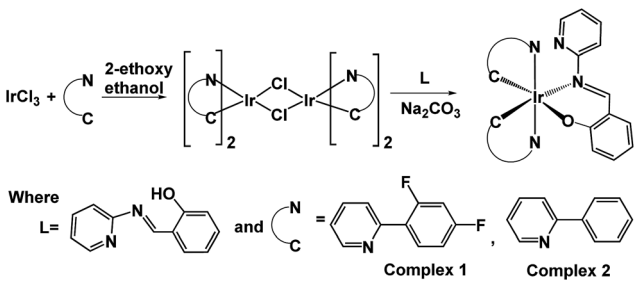

Scheme 1 Schematic representation of synthetic routes for complexes **1** and **2**.

7.00 (ddd, $J = 9.6, 6.7, 2.7$ Hz, 1H), 6.87 (dd, $J = 11.2, 3.7$ Hz, 1H), 6.83–6.68 (m, 3H), 6.58 (t, $J = 6.9$ Hz, 1H), 6.49–6.32 (m, 2H), 6.18 (d, $J = 7.5$ Hz, 1H), 6.05 (d, $J = 7.4$ Hz, 1H), 5.86 (d, $J = 8.0$ Hz, 1H). ESI-HRMS calculated: $C_{34}H_{26}IrN_4O$ ($[M + H]^+$): m/z, 699.1736, found; ($[M + H]^+$): m/z, 699.2612, pale red solid; yield, 50.00% (Fig. S3†).

Fabrication of thin-films on substrate for PL measurements

A 10^{-3} M solution of each of the complexes (in THF) was prepared. 2–3 drops of these solutions were placed on thin glass substrates (2×2 cm^2). The solvent was allowed to evaporate slowly.

X-ray single crystal diffraction study

Single crystal X-ray diffraction data for **2** was recorded on a Bruker AXS KAPPA APEX-II CCD and a Rigaku[54] Mercury 375/M CD (XtaLAB mini) diffractometer respectively by using graphite Monochromated Mo-K_α radiation at 100.0(1) K with an Oxford cryosystem. The data sets collected on Bruker AXS KAPPA APEX-II Kappa were collected using Bruker APEX-II suite, data reduction and integration were performed by SAINT V7.685A12 (Bruker AXS, 2009) and absorption corrections and scaling was done using SADABS V2008/112 (Bruker AXS). The data sets, which were collected on XtaLAB mini diffractometer, were processed with Rigaku Crystal Clear suite 2.0. The crystal structures were solved by using SHELXS2013 (ref. 55) and were refined using SHELXL2013 available within Olex2.[56] All the hydrogen atoms have been geometrically fixed and refined using the riding model except the hydride anion, coordinating the iridium(III) atom, which has been located from the difference Fourier map and refined isotropically. All the diagrams have been generated using Mercury 3.1.1.[57] Geometric calculations have been done using PARST.[58]

MTT assay

For determining the *in vitro* cytotoxicity, HOS cells (obtained from NCCS Pune) cultured in minimum essential media (Hi media, # 41500-067) containing 10% FBS (Invitrogen, #26140-079) and 1% penicillin-streptomycin mixture (Invitrogen, # 10378-016) were grown in log phase. Cells were then seeded at a density of 4000 cells per well in 96 well plate and incubated overnight with 5% CO_2 at 37 °C. The next day **2** was added at concentrations – 1 μM, 2 μM, 5 μM, 10 μM, 15 μM, 20 μM, 25 μM, 30 μM (in triplicates) diluted with DMSO (SDFCL, # 20323 L05) for 24 h with respective control where no compound was added. Following treatment, MTT (Stock concentration 5 mg mL^{-1}) (MTT: Sigma, #M5655) 20 μL was added and incubated for 4 h post which formazan crystals were solubilized using DMSO and readings were obtained at 495 nm with a differential filter at 690 nm using an enzyme-linked immune-sorbent assay (ELISA) micro-plate reader (Start-fax 2100).

Percentage of viable cells was calculated using the following formula:

$$\text{Viability (\%)} = (\text{mean absorbance value of drug treated cells})/(\text{mean absorbance value of control}) \times 100$$

Cell imaging

For the bio-imaging experiment, HOS cells were seeded at a density of 2×10^4 per cover slip and incubated with 5% CO_2 at 37 °C for 24 h. Following incubation, **2** dissolved in DMSO (25 μM) was added to the cells grown on a coverslip and kept inside the incubator for another 24 h. Cells were then fixed in chilled methanol for 10 min at −20 °C, counter stained with DAPI (0.2 μg mL^{-1}, Sigma), and incubated for 10 min followed by three PBS washes. Coverslips were then mounted with glycerol on glass slide and observed at 100× under a fluorescence microscope (OLYMPUS, U-25ND25).

To study the organelle specific localization of **2**, mitochondrial staining was done. Cells grown in a coverslip which were pre-treated as above with **2** for 24 hours. Mito Tracker (RedFM, Invitrogen # M22425) was added at a concentration of 300 nM μL^{-1} in serum free media and incubated at 37 °C for 30 min followed by three PBS washes. Cells were then fixed in 4% paraformaldehyde (in PBS) and incubated at 37 °C for 15 minutes. Following fixation cells were washed several times with PBS followed by glycerol mounting and observation under fluorescence microscope.

Measurement of ROS generation

The generation of ROS was measured using the cell-permeable fluorescent dye 2′-7′-dichlorofluorescein-diacetate (H2DCFDA) (Sigma-Aldrich, USA), a non-fluorescent compound, which is converted into highly fluorescent dichloro-fluorescein (DCF) by cellular peroxides. Briefly, HOS cells were exposed to the **2** for the indicated times and then were loaded with H2DCFDA (20 μM) dissolved in PBS. Following incubation at 37 °C for 1 h, the cells were washed with PBS and fluorescence was monitored with a fluorimeter (Fluroskan Asent, Thermo Scientific) at an excitation wavelength of 485 nm and emission wavelength of 530 nm. The fluorescence emitted by untreated cells loaded with DCF-DA was taken as a control and the treated values were plotted accordingly.

Results and discussion

Complexes **1** and **2** were characterized by ^{1}H NMR, HRMS and SXRD. The ^{1}H signal of the imine C–H group shifts to $\delta =$ 8.28 ppm and 8.34 ppm for **1** and **2**, respectively, with respect to the signal obtained for the pristine ligand 2-((pyridin-2-ylimino) methyl)phenol ($\delta = 9.46$ ppm). The ^{19}F NMR shows four doublet signals in between $-108.67 < \delta < -111.77$ ppm because of F–F coupling. The HRMS spectrum exhibits major fragments as $[M + H]^+$ at m/z 771.1331 and 699.2612 for **1** and **2**, respectively. Furthermore, complex **2** has been authenticated by SXRD (Fig. 1).

Photophysical properties in solution

The UV-vis absorption spectra of **1** and **2** were recorded in degassed DCM. Absorbance profiles show an intense absorption band at *ca.* 270–310 nm that our electronic structure calculations assign to ligand-centered (LC) and charge transfer (CT) transitions involving ppy and Schiff base (SB) ligands, moderate bands at 330–450 nm corresponding to ^{1}MLCT (d(Ir) → π*(ppy or SB)),

^{1}MLLCT (d(Ir) + π(SB) → π*(ppy)) and ^{1}MLCT/LC states (d(Ir) + π(SB) → π*(SB)) and a less intense tailing band beyond 450 nm that can be attributed to spin-forbidden transitions of mainly ^{3}MLCT character (Fig. 2). Similar absorption spectra were observed in different organic solvents (Fig. S5†). However, the solid state absorption spectra of both the complexes showed a broad absorbance band in the visible range (400–520 nm) (Fig. S4†). These complexes are almost non emissive under excitation at 365 nm in organic solvents at ambient temperature. The recorded phosphorescent emission spectra of **1** in degassed DCM showed an emission with $\lambda_{max} = 495$ nm, while **2** exhibited a λ_{max} at 515 nm at room temperature.

DFT based calculations indicate that the lowest emissive triplet state of complexes **1** and **2** can be described as the single electron occupation of the ground state HOMO, obtained as a combination of a d-orbital on the iridium atom and π-orbital of the Schiff base (L) ligand, and the LUMO+1, corresponding to a π* orbital centered on the L ligand (Fig. 3). Therefore, the phosphorescent states of **1** and **2** can be qualitatively described as mixed metal-to-ligand charge transfer and ligand centered (^{3}MLCT/^{3}LC).

Further, the emission spectra of complex **2** did not show an obvious change in presence of different organic solvents. These facts suggest that the lowest excited state of **2** is of predominantly LC character along with a lesser contribution from MLCT states (Fig. S6†).

Aggregation induced emission

The very weak emission intensities observed for complexes **1** and **2** in common organic solvents increase significantly upon aggregation. The solid state emission spectra of **1** and **2** show a red shifted emission with respect to the emission band recorded in solution and found at 600 nm and 610 nm, respectively (Fig. S7†). The AIE effect for these complexes is investigated using solvent mixtures with different fractions of water (f_w) and methanol. The maximum PL intensity for **1** and **2** is recorded at $f_w = 90$, which is ~125 and ~950 times higher than for pure methanol solutions, respectively. The observed PL maxima of **1** at 495 nm in methanol shifts to 581 nm at $f_w = 95\%$ (Fig. 4), while the maximum emission of **2** was found at 515 nm in methanol and at 605 nm for $f_w = 95\%$ (Fig. 5). The large red shifted emission in aggregated or solid state in comparison to solution state may be attributed to π–π stacking in adjacent phenyl pyridine rings (Fig. 6b).

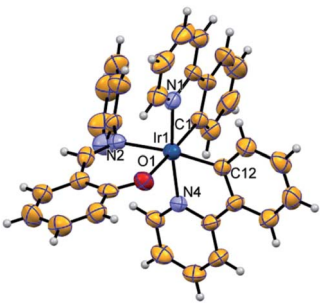

Fig. 1 ORTEP diagram of structure **2** drawn using 50% probability ellipsoid, showing the octahedral coordination geometry for iridium(III).

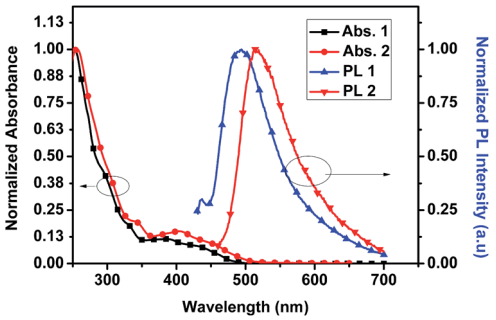

Fig. 2 UV-visible absorption and photoluminescence spectra of **1** and **2** in 1×10^{-5} M DCM.

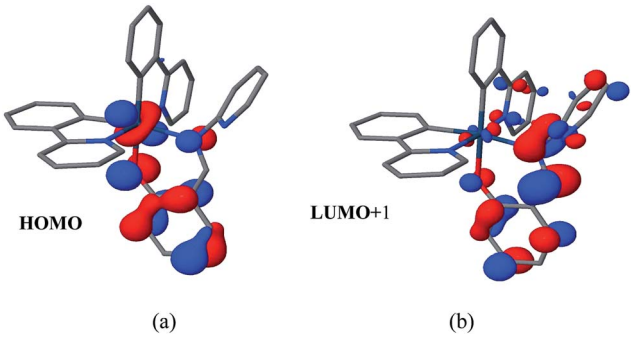

Fig. 3 (a) HOMO and (b) LUMO+1 of complex **2** corresponding to the molecular orbitals bearing the unpaired electrons in the lowest triplet state.

In order to get some insight into the weak interactions that are present in the aggregated state we used the crystal structure of **2** as a qualitative reference. Analyzing the crystal packing in crystals of **2** different types of short contacts (C–H···π and C–H···N) in the range of 2.37–2.80 Å, are evident. The causes of AIE in bis cyclometalated iridium(III) salicylaldimine complexes has been controversial[46,47] but a recent paper[59] has clarified the mechanism involving restriction of a tilting motion of the salicylimine ligand in the aggregated state. An additional π–π interaction between two fused aromatic rings is also observed at a distance of 3.85 Å between ring centroids (Fig. 6). The presence of all these interactions enforce molecular rigidity in the solid state, enhancing the efficiency of RIM processes blocking the non radiative deactivation of the emitting state with the overall result of a strong emission in solid and aggregated states. The sizes of nanoaggregates for **1** and **2** at $f_w = 90\%$ have been measured by dynamic light scattering (DLS) and the results indicate the formation of particles in the range of 350–395 nm and 410–476 nm, respectively (Fig. S8†). The aggregate formation was further supported by absorption spectra recorded in different water fraction (f_w) resulted a level-off tail (at $f_w = 90\%$) in the longer wavelength region (400–650 nm) (Fig. S9†). However, the

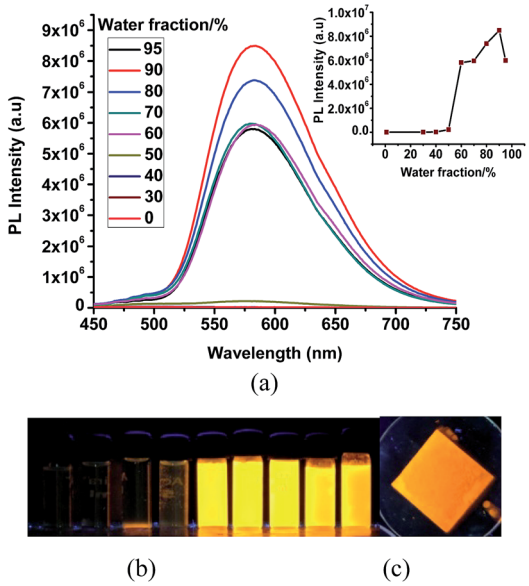

Fig. 4 (a) PL spectra of **1** in MeOH/water mixed solvents with different f_w (water fraction). Inset: variation of the PL intensity with respect to water contents. (b) Luminescent images of **1** in solutions with different water fractions (c) image for a solid sample of **1** under irradiation with a 365 nm UV lamp [$c = 10 \times 10^{-5}$ M].

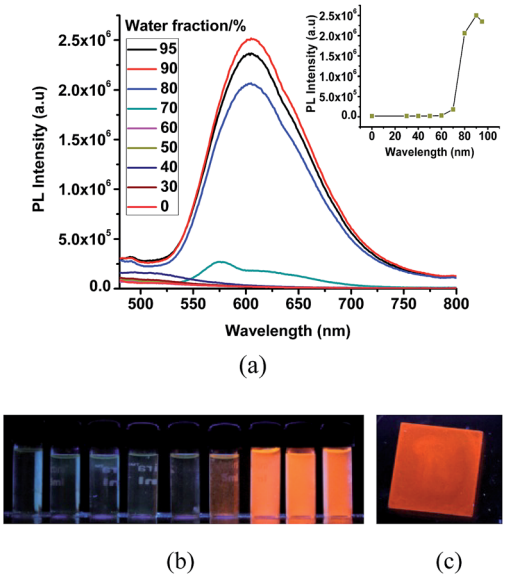

Fig. 5 (a) PL spectra of **2** in MeOH/water mixed solvents with different f_w (water fraction). Inset: variation of PL intensity with respect to different water fraction. (b) Luminescent images of **2** in different water fraction (c) image for a solid sample of **2** under irradiation with a 365 nm UV lamp; [$c = 10 \times 10^{-5}$ M].

recorded excitation spectra at different f_w showed major peak in the range of 350–370 nm (Fig. S10†).

The absolute PL quantum yields for **1** and **2** have been found to be 6.39% and 6.03%, which are almost ~60 times and ~35 times higher than in solution, respectively. These observations support the remarkable AIE nature of these complexes.

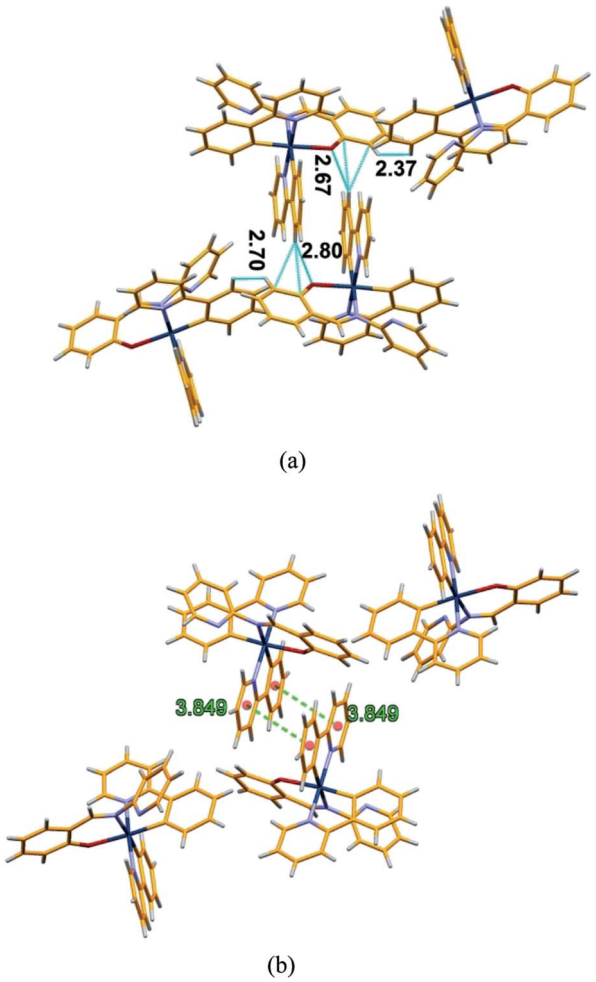

Fig. 6 (a) Packing diagram of **2** showing the different short contacts (b) packing diagram of **2** showing π–π stacking interaction between aromatics ring.

Effect of iridium complex on cell viability of osteosarcoma cells

HOS cells were treated (detail treatment was described in materials and methods) with **2** for 24 h and then the cell viability was determined. As shown in Fig. 7, **2** inhibited the cell viability of HOS cell line in a dose-dependent manner. The IC50 of the compound was found to be around 25 μM. The compound showed cytotoxicity only at higher concentrations. In association to the reduced cytotoxicity shown by these compounds, we did not observe a significant increase in reactive oxygen species levels upon exposure of the cells with the compound (data not shown). It is worth mentioning here that many anti-cancer agents induce apoptosis mediated cell death in cancer cells by an increase in cellular ROS levels.

This provided us with the hint that these compounds can be effectively used for bio-imaging purposes. Hence, this complex was successfully applied in bio-imaging. The complex **2** was successfully internalized by the cells and being an AIE compound, the complex following incubation with cancer cells

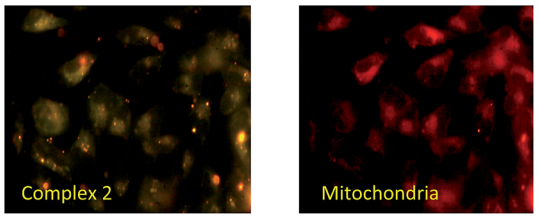

Fig. 7 Bio-imaging of HOS cells after 24 h incubation with complex 2 then counter stained with Mito Tracker to check the localization of compound, magnification 100×. Scale bar (5 μm).

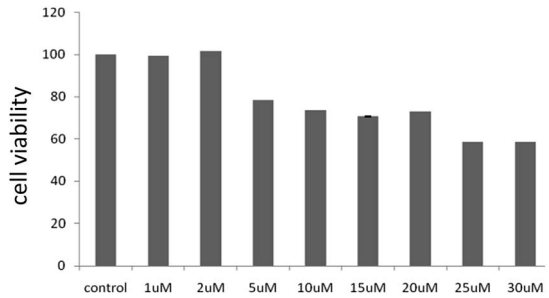

Fig. 8 Cytotoxicity assay for 2 in human osteosarcoma cells, HOS after 24 h of incubation.

exhibited good fluorescence inside the cells depicting high cell membrane permeability and AIE properties (Fig. 7). The compound though entered the cells, but was not able to enter the nucleus. We were therefore interested in knowing the probable sub-cellular localization of the aggregated compound. A mitochondrial staining with commercially available fluorescent dye, Mito Tracker showed co-localization of the AIE-induced fluorescence and mitochondrial dye emitted fluorescence (Fig. 7). Due to its comparatively low cytotoxicity (Fig. 8), cellular internalization property and enhanced AIE characteristics this compound can be a potential bio-imaging agent. Future studies directed towards functionalization of this compound with specifically cancer cell targeting moieties, like folic acid can have huge impact on cancer diagnostics and treatment.

Conclusions

We have reported the synthesis and characterization of two new AIE active iridium(III) complexes with using a simple Schiff base type supporting ligand. From the mechanistic point of view, the AIE effect is suggested to originate from restriction of internal motion (RIM) consistent with previous studies.[59] Finally, complex 2 has been successfully employed as a bioimaging probe, which selectively stain the mitochondria.

Acknowledgements

We thank the 'Department of Science and Technology (DST)' and 'Council of Scientific and Industrial Research (CSIR)', Govt. of India to support this work financially under the following projects with project numbers, SB/S1/IC-13/2014 and 01/2551/12/EMR-II, respectively. The 'UGC-SAP' and DST-FIST program for the chemistry department has been acknowledged for instrumental support. This work has also been supported by the Basque Government (project IT588-13) and the Spanish Government (project CTQ2015-64579-C3-3-P). D. C. thanks IKERBASQUE, Basque Foundation for Science, for financial support. C. C. is indebted to the Spanish 'Ministerio de Economía y Competitividad' for a predoctoral FPI grant.

Notes and references

1 Y. Chen, L. Qiao, B. Yu, G. Li, C. Liu, L. Ji and H. Chao, *Chem. Commun.*, 2013, **49**, 11095–11097.
2 B. Wang, Y. Liang, H. Dong, T. Tan, B. Zhan, J. Cheng, K. K.-W. Lo, Y. W. Lam and S. H. Cheng, *ChemBioChem*, 2012, **13**, 2729–2737.
3 Y. You, *Curr. Opin. Chem. Biol.*, 2013, **17**, 699–707.
4 Q. Zhao, C. Huang and F. Li, *Chem. Soc. Rev.*, 2011, **40**, 2508–2524.
5 J. A. Kanis, D. Black, C. Cooper, P. Dargent, B. Dawson-Hughes, C. D. Laet, P. Delmas, J. Eisman, O. Johnell, B. Jonsson, L. Melton, A. Oden, S. Papapoulos, H. Pols, R. Rizzoli, A. Silman and A. Tenenhouse, *Osteoporosis Int.*, 2002, **13**, 527–536.
6 W. J. Strittmatter, A. M. Saunders, D. Schmechel, M. Pericak-Vance, J. Enghild, G. S. Salvesen and A. D. Roses, *Proc. Natl. Acad. Sci. U. S. A.*, 1993, **90**, 1977–1981.
7 E. V. Loftus Jr, *Gastroenterology*, 2004, **126**, 1504–1517.
8 H. Cai and D. G. Harrison, *Circ. Res.*, 2000, **87**, 840–844.
9 K. K.-W. Lo, A. W.-T. Choi and W. H.-T. Law, *Dalton Trans.*, 2012, **41**, 6021–6047.
10 Y. Li, C.-P. Tan, W. Zhang, L. He, L.-N. Ji and Z.-W. Mao, *Biomaterials*, 2015, **39**, 95–104.
11 P. K. Sasmal, C. N. Streu and E. Meggers, *Chem. Commun.*, 2013, **49**, 1581–1587.
12 S. P.-Y. Li, C. T.-S. Lau, M.-W. Louie, Y.-W. Lam, S. H. Cheng and K. K.-W. Lo, *Biomaterials*, 2013, **34**, 7519–7532.
13 R. Cao, J. Jia, X. Ma, M. Zhou and H. Fei, *J. Med. Chem.*, 2013, **56**, 3636–3644.
14 W. Pendergrass, N. Wolf and M. Poot, *Cytometry, Part A*, 2004, **61**, 162–169.
15 G. V. Bünau, *Ber. Bunsen-Ges. Phys. Chem.*, 1970, **74**, 1294–1295.
16 J. Luo, Z. Xie, J. W. Y. Lam, L. Cheng, H. Chen, C. Qiu, H. S. Kwok, X. Zhan, Y. Liu, D. Zhu and B. Z. Tang, *Chem. Commun.*, 2001, 1740–1741, DOI: 10.1039/b105159h.
17 Z. Zhao, B. He and B. Z. Tang, *Chem. Sci.*, 2015, **6**, 5347–5365.
18 H. Wang, E. Zhao, J. W. Y. Lam and B. Z. Tang, *Mater. Today*, 2015, **18**, 365–377.
19 Y. Hong, J. W. Y. Lam and B. Z. Tang, *Chem. Commun.*, 2009, 4332–4353, DOI: 10.1039/b904665h.
20 J. Mei, N. L. C. Leung, R. T. K. Kwok, J. W. Y. Lam and B. Z. Tang, *Chem. Rev.*, 2015, **115**, 11718–11940.
21 P. Alam, V. Kachwal and I. R. Laskar, *Sens. Actuators, B*, 2016, **228**, 539–550.

22 W. Z. Yuan, Y. Gong, S. Chen, X. Y. Shen, J. W. Y. Lam, P. Lu, Y. Lu, Z. Wang, R. Hu, N. Xie, H. S. Kwok, Y. Zhang, J. Z. Sun and B. Z. Tang, *Chem. Mater.*, 2012, **24**, 1518–1528.
23 E. Wang, J. W. Y. Lam, R. Hu, C. Zhang, Y. S. Zhao and B. Z. Tang, *J. Mater. Chem. C*, 2014, **2**, 1801–1807.
24 X. Zhang, J. Ye, L. Xu, L. Yang, D. Deng and G. Ning, *J. Lumin.*, 2013, **139**, 28–34.
25 Y. Zhang, H. Li, G. Zhang, X. Xu, L. Kong, X. Tao, Y. Tian and J. Yang, *J. Mater. Chem. C*, 2016, **4**, 2971–2978.
26 R. T. K. Kwok, C. W. T. Leung, J. W. Y. Lam and B. Z. Tang, *Chem. Soc. Rev.*, 2015, **44**, 4228–4238.
27 J. Mei, Y. Hong, J. W. Y. Lam, A. Qin, Y. Tang and B. Z. Tang, *Adv. Mater.*, 2014, **26**, 5429–5479.
28 N. L. C. Leung, N. Xie, W. Yuan, Y. Liu, Q. Wu, Q. Peng, Q. Miao, J. W. Y. Lam and B. Z. Tang, *Chem.–Eur. J.*, 2014, **20**, 15349–15353.
29 Y. Chen, M. Li, Y. Hong, J. W. Y. Lam, Q. Zheng and B. Z. Tang, *ACS Appl. Mater. Interfaces*, 2014, **6**, 10783–10791.
30 J. Liang, H. Shi, R. T. K. Kwok, M. Gao, Y. Yuan, W. Zhang, B. Z. Tang and B. Liu, *J. Mater. Chem. B*, 2014, **2**, 4363–4370.
31 R. Hu, E. Lager, A. Aguilar-Aguilar, J. Liu, J. W. Y. Lam, H. H. Y. Sung, I. D. Williams, Y. Zhong, K. S. Wong, E. Peña-Cabrera and B. Z. Tang, *J. Phys. Chem. C*, 2009, **113**, 15845–15853.
32 P. Alam, I. R. Laskar, C. Climent, D. Casanova, P. Alemany, M. Karanam, A. R. Choudhury and J. Raymond Butcher, *Polyhedron*, 2013, **53**, 286–294.
33 P. Alam, C. Climent, G. Kaur, D. Casanova, A. Roy Choudhury, A. Gupta, P. Alemany and I. R. Laskar, *Cryst. Growth Des.*, 2016, **16**, 5738–5752.
34 D. Kourkoulos, C. Karakus, D. Hertel, R. Alle, S. Schmeding, J. Hummel, N. Risch, E. Holder and K. Meerholz, *Dalton Trans.*, 2013, **42**, 13612–13621.
35 C.-H. Yang, M. Mauro, F. Polo, S. Watanabe, I. Muenster, R. Fröhlich and L. De Cola, *Chem. Mater.*, 2012, **24**, 3684–3695.
36 K. Zhang, S. Liu, Q. Zhao, F. Li and W. Huang, in *Luminescent and Photoactive Transition Metal Complexes as Biomolecular Probes and Cellular Reagents*, ed. K. K.-W. Lo, Springer, Berlin Heidelberg, 2015, vol. 165, ch. 166, pp. 131–180.
37 R. D. Costa, E. Ortí, H. J. Bolink, F. Monti, G. Accorsi and N. Armaroli, *Angew. Chem., Int. Ed.*, 2012, **51**, 8178–8211.
38 Y. Zhou and J. Yoon, *Chem. Soc. Rev.*, 2012, **41**, 52–67.
39 J. F. Zhang, Y. Zhou, J. Yoon and J. S. Kim, *Chem. Soc. Rev.*, 2011, **40**, 3416–3429.
40 P. Alam, M. Karanam, D. Bandyopadhyay, A. R. Choudhury and I. R. Laskar, *Eur. J. Inorg. Chem.*, 2014, **2014**, 3710–3719.
41 S. Lamansky, P. Djurovich, D. Murphy, F. Abdel-Razzaq, H.-E. Lee, C. Adachi, P. E. Burrows, S. R. Forrest and M. E. Thompson, *J. Am. Chem. Soc.*, 2001, **123**, 4304–4312.
42 P. Alam, G. Kaur, A. Sarmah, R. K. Roy, A. R. Choudhury and I. R. Laskar, *Organometallics*, 2015, **34**, 4480–4490.
43 P. Alam, P. Das, C. Climent, M. Karanam, D. Casanova, A. R. Choudhury, P. Alemany, N. R. Jana and I. R. Laskar, *J. Mater. Chem. C*, 2014, **2**, 5615–5628.
44 P. Alam, G. Kaur, S. Chakraborty, A. Roy Choudhury and I. R. Laskar, *Dalton Trans.*, 2015, **44**, 6581–6592.
45 P. Alam, G. Kaur, C. Climent, S. Pasha, D. Casanova, P. Alemany, A. Roy Choudhury and I. R. Laskar, *Dalton Trans.*, 2014, **43**, 16431–16440.
46 K. Huang, H. Wu, M. Shi, F. Li, T. Yi and C. Huang, *Chem. Commun.*, 2009, 1243–1245, DOI: 10.1039/B816056B.
47 Q. Zhao, L. Li, F. Li, M. Yu, Z. Liu, T. Yi and C. Huang, *Chem. Commun.*, 2008, 685–687, DOI: 10.1039/b712416c.
48 Y. You, H. S. Huh, K. S. Kim, S. W. Lee, D. Kim and S. Y. Park, *Chem. Commun.*, 2008, 3998–4000, DOI: 10.1039/b806541a.
49 A. D. Becke, *J. Chem. Phys.*, 1993, **98**, 5648–5652.
50 P. J. Hay and W. R. Wadt, *J. Chem. Phys.*, 1985, **82**, 270–283.
51 W. R. Wadt and P. J. Hay, *J. Chem. Phys.*, 1985, **82**, 284–298.
52 P. J. Hay and W. R. Wadt, *J. Chem. Phys.*, 1985, **82**, 299–310.
53 M. J. Frisch, G. W. Trucks, H. B. Schlegel, G. E. Scuseria, M. A. Robb, J. R. Cheeseman, G. Scalmani, V. Barone, B. Mennucci, G. A. Petersson, H. Nakatsuji, M. Caricato, X. Li, H. P. Hratchian, A. F. Izmaylov, J. Bloino, G. Zheng, J. L. Sonnenberg, M. Hada, M. Ehara, K. Toyota, R. Fukuda, J. Hasegawa, M. Ishida, T. Nakajima, Y. Honda, O. Kitao, H. Nakai, T. Vreven, J. A. Montgomery Jr, J. E. Peralta, F. Ogliaro, M. J. Bearpark, J. Heyd, E. N. Brothers, K. N. Kudin, V. N. Staroverov, R. Kobayashi, J. Normand, K. Raghavachari, A. P. Rendell, J. C. Burant, S. S. Iyengar, J. Tomasi, M. Cossi, N. Rega, N. J. Millam, M. Klene, J. E. Knox, J. B. Cross, V. Bakken, C. Adamo, J. Jaramillo, R. Gomperts, R. E. Stratmann, O. Yazyev, A. J. Austin, R. Cammi, C. Pomelli, J. W. Ochterski, R. L. Martin, K. Morokuma, V. G. Zakrzewski, G. A. Voth, P. Salvador, J. J. Dannenberg, S. Dapprich, A. D. Daniels, Ö. Farkas, J. B. Foresman, J. V. Ortiz, J. Cioslowski and D. J. Fox, *Gaussian 09, Revision E 01, Gaussian, Inc.*, Wallingford, CT, 2009.
54 *CrystalClear 2.0*, Rigaku Corporation, Tokyo, Japan, 2016.
55 G. Sheldrick, *Acta Crystallogr., Sect. A: Found. Crystallogr.*, 2008, **64**, 112–122.
56 O. V. Dolomanov, L. J. Bourhis, R. J. Gildea, J. A. K. Howard and H. Puschmann, *J. Appl. Crystallogr.*, 2009, **42**, 339–341.
57 A. Spek, *Acta Crystallogr., Sect. D: Biol. Crystallogr.*, 2009, **65**, 148–155.
58 M. Nardelli, *J. Appl. Crystallogr.*, 1995, **28**, 659.
59 A. J. Howarth, R. Patia, D. L. Davies, F. Lelj, M. O. Wolf and K. Singh, *Eur. J. Inorg. Chem.*, 2014, **2014**, 3657–3664.